

Measurement of Mechanical Coherency Temperature and Solid Volume Fraction in Al-Zn Alloys Using *In Situ* X-ray Diffraction During Casting



JEAN-MARIE DREZET, BASTIEN MIREUX, GÜVEN KURTULDU,
OXANA MAGDYSYUK, and MICHAEL DRAKOPOULOS

During solidification of metallic alloys, coalescence leads to the formation of solid bridges between grains or grain clusters when both solid and liquid phases are percolated. As such, it represents a key transition with respect to the mechanical behavior of solidifying alloys and to the prediction of solidification cracking. Coalescence starts at the coherency point when the grains begin to touch each other, but are unable to sustain any tensile loads. It ends up at mechanical coherency when the solid phase is sufficiently coalesced to transmit macroscopic tensile strains and stresses. Temperature at mechanical coherency is a major input parameter in numerical modeling of solidification processes as it defines the point at which thermally induced deformations start to generate internal stresses in a casting. This temperature has been determined for Al-Zn alloys using *in situ* X-ray diffraction during casting in a dog-bone-shaped mold. This setup allows the sample to build up internal stress naturally as its contraction is prevented. The cooling on both extremities of the mold induces a hot spot at the middle of the sample which is irradiated by X-ray. Diffraction patterns were recorded every 0.5 seconds using a detector covering a $426 \times 426 \text{ mm}^2$ area. The change of diffraction angles allowed measuring the general decrease of the lattice parameter of the fcc aluminum phase. At high solid volume fraction, a succession of strain/stress build up and release is explained by the formation of hot tears. Mechanical coherency temperatures, 829 K to 866 K (556 °C to 593 °C), and solid volume fractions, ca. 98 pct, are shown to depend on solidification time for grain refined Al-6.2 wt pct Zn alloys.

DOI: 10.1007/s11661-015-3041-y

© The Minerals, Metals & Materials Society and ASM International 2015

I. INTRODUCTION

COALESCENCE corresponds to the formation of solid bridges between grains when both solid and liquid phases are percolated.^[1] As such, it represents a key transition in the solidification of metallic alloys. Coalescence starts at the coherency point when the grains begin to touch each other, but are unable to sustain any tensile loads. Rappaz *et al.*^[2] have used the concept of disjoining-pressure used in fluid dynamics to establish a theoretical framework for the coalescence of primary phase dendritic arms within a single grain or at grain boundaries. The authors have shown that for pure substances, approaching planar liquid/solid interfaces coalesce to a grain boundary at an undercooling ΔT_b

that is proportional to the difference between the grain boundary energy and two times the solid/liquid interfacial energy.^[2] The latter quantity depends on the grain misorientation. When this quantity is positive, the two liquid/solid interfaces are “repulsive.” In this case, a stable liquid film between adjacent dendrite arms located across such grain boundaries can remain until the undercooling exceeds ΔT_b .

For alloys, coalescence is also influenced by the concentration of solute elements in the liquid films.^[2] The temperature and concentration of the liquid films must reach a coalescence line parallel to, but ΔT_b below, the liquidus line before coalescence can occur.

At the macroscopic level, *i.e.*, at the level of many randomly oriented grains, coalescence must be considered as a transition taking place between coherency (first contact between the grains) and rigidity (ability to transmit tensile strains and stresses), also called mechanical coherency^[3] or tensile coherency.^[4] If coalescence between some grains is slowed down, *i.e.*, finishes at lower temperatures, the mushy structure becomes particularly sensitive to hot tearing or solidification cracking.^[5] This defect is a spontaneous failure of semi-solid metallic alloys that results in an intergranular fracture profile. It forms during casting near the end of solidification where straining becomes localized and local liquid permeability is very low. Coalescence ends at the

JEAN-MARIE DREZET, MER Professor, and BASTIEN MIREUX, Post Doctoral Fellow, are with Computational Materials Laboratory, Ecole Polytechnique Federale Lausanne, Station 12, Lausanne 1015, Switzerland. Contact e-mail: jean-marie.drezet@epfl.ch OXANA MAGDYSYUK, Support Scientist, and MICHAEL DRAKOPOULOS, Beam Line Scientist, are with the RAL, Diamond Light Source, Didcot, UK. GÜVEN KURTULDU, formerly Postdoctoral Fellow with the Computational Materials Laboratory, Ecole Polytechnique Federale Lausanne, is now Postdoctoral Fellow with the Laboratory of Metal Physics and Technology, Department of Materials, ETH Zürich, 8093 Zurich, Switzerland.

Manuscript submitted March 13, 2015.

Article published online July 9, 2015

rigidity point when the structure is able to sustain substantial tensile strains and stresses, *i.e.*, when the solid phase is sufficiently percolated to bear tensile loads. The rigidity temperature is important as it determines the very instant macroscopic stresses start to build up owing to thermally induced deformations.^[6] It is an important input data for numerical modeling of as-cast residual stresses in billets and rolling sheet ingots as it dictates the temperature below which thermal strains start to occur.

The mechanical behavior of alloys in the mushy state has recently been intensively studied using X-ray microtomography.^[7-13] *In situ* tensile test experiments were performed by Terzi *et al.*^[7,8] on Al-Cu alloys in the mushy state at the European Synchrotron Radiation Facility (ESRF). The major drawbacks of such *in situ* tensile tests are that they are carried out in isothermal conditions, and not during rapid cooling, since the time resolution for X-ray microtomography imaging is still limited.^[9] Moreover, the exact mechanical loading within the material is not known as the deformation, localized in the specimen at the high temperature region, is not measured. These tests are presently limited to Al-Cu alloys^[10] in order to get a good contrast between the liquid and solid phases, and the alloy is tested after heating to the correct temperature within the solidification interval and not during solidification from the fully liquid state. The last point is particularly detrimental as solidifying microstructures are different from those obtained after heating owing to dendrite coarsening and redistribution of solute elements.^[11]

Neutron diffraction has been used to measure post mortem internal stresses in as-cast billet^[14] and as-quenched thick plates.^[15] Robinson *et al.*^[16] have measured the influence of quenching and aging on rectilinear AA7449 forged blocks. With these studies, neutron diffraction at high flux sources appeared to be particularly well suited for stress measurements in aluminum alloys as this metal is very transparent to neutrons. On the other hand, *in situ* studies of stress accumulation in solidifying metals are rather limited. Woo *et al.*^[17] published in 2007 a study on *in situ* neutron diffraction measurements of stresses during friction stir welding of 6061-T6 aluminum alloy. Neutrons were also used to determine *in situ* the very moment when macroscopic strains and stresses appear in the mushy alloy.^[3] As one diffraction peak was recorded only every 11 seconds, the cooling rate was reduced and rigidity temperatures were measured in grain refined Al-Cu 13 wt pct alloys. The hot tearing tendency was linked to the rigidity temperature, higher or equal to the eutectic temperature, the cooling rate, and the degree of primary phase grain percolation.

In the current study, X-ray diffraction (XRD) has been performed *in situ* during solidification with a higher time resolution at I12 high-energy beamline in Diamond Light Source, UK.^[18] Rigidity temperature has been measured in Al-Zn alloys under various cooling regimes in a dog-bone-shaped mold similar to the neutron experiments, where solidification and tensile straining are concomitant. This situation is similar to the centre-line of DC cast aluminum billets where hot tears are

known to form.^[19] Al-Zn alloys are particularly interesting as they are the base of the 7xxx aluminum alloys series. Those alloys are known to be very sensitive to hot cracking^[20] owing to their long freezing range.

II. *IN SITU* X-RAY DIFFRACTION DURING CASTING

A. *Materials and Castings*

Al-5 wt pct Zn alloys were prepared by melting high purity aluminum and pure zinc in a stainless steel crucible at 993 K (720 °C). The alloys were then grain refined with 0.4 wt pct Al-TiB₂ master alloy. The casting into a dog-bone-shaped mold with water-cooled extremities and subsequent solidification was carried out in sync with the *in situ* acquisition of XRD patterns. Three different solidification times were tested by adjusting the water debit and the initial mold temperature. The mold, shown in Figure 1, is usually used to study the hot tearing susceptibility of new alloys. Its length is adjustable varying from 70 to 110 mm. The height of the casting is around 15 mm, its thickness ca 7.5 mm, and the length of the casting ends is 40 mm. A small taper eases the extraction of the casting. A hot spot forms at the very center of the casting as cooling conditions are similar at both ends. The axial contraction of the casting is prevented by the steel central part. The thermal contraction of the solidifying material is constrained and stresses developing at the hot spot may lead to hot cracking. The major advantage of this configuration is that solidification and tensile straining are concomitant. The amount of straining on the hot spot is controlled by modulating cooling of the mold extremities, by preheating the mold using electric heating elements and by changing the length of the central part of the mold, *i.e.*, by changing the amount of straining that is localized at the hot spot.^[3]

B. *In Situ X-ray Diffraction*

In order to measure the accumulation of elastic strain and thus of stress during casting, the lattice spacing was measured *in situ* at the hot spot location using XRD. Small conical holes were machined in the steel mold to provide unimpeded access to the sample for the X-ray beam. Insulating alumina muffles were used to plug these holes to avoid any liquid metal leakage. As shown in Figure 1(b), the crucible was mounted on a tilting support in order to control the pouring remotely by a pneumatic pusher. This allowed us to synchronize the onset of the acquisition of diffraction data precisely with the process of pouring.

Six type K thermocouples arrayed along the sample axis within the casting allowed linking the temperature within the gage volume with the formation and shift of the diffraction peaks during solidification. Precisely, one $\phi = 0.5$ mm thermocouple was partially in the hot spot, while the remaining five thermocouples were placed along the remaining length of the dog-bone.

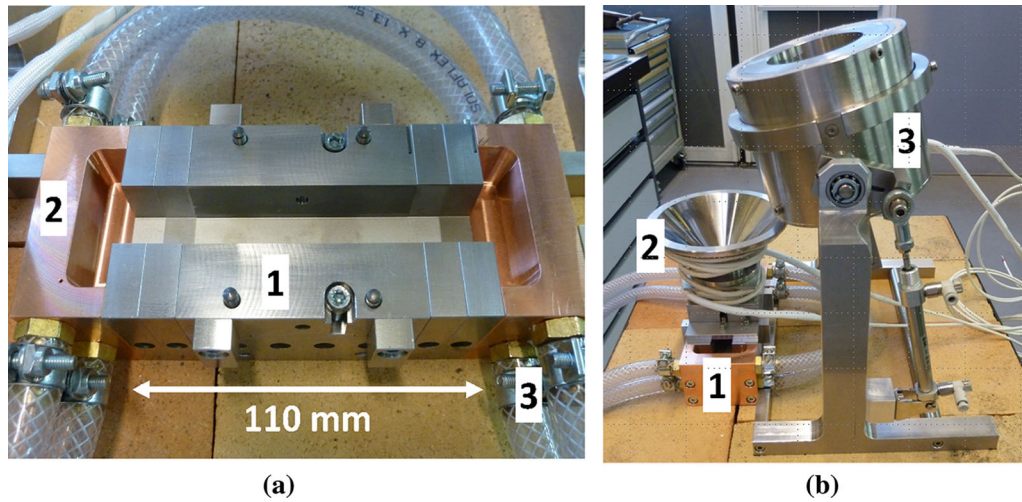


Fig. 1—(a) Dog-bone-shaped mold (1) with the two X-ray windows within the mold to let the X-ray beam penetrate the solidifying alloy, water-cooled copper chills (2) and water pipes (3), (b), experimental setup showing the instrumented mold (1), the tundish (2) and the rotating crucible (3).

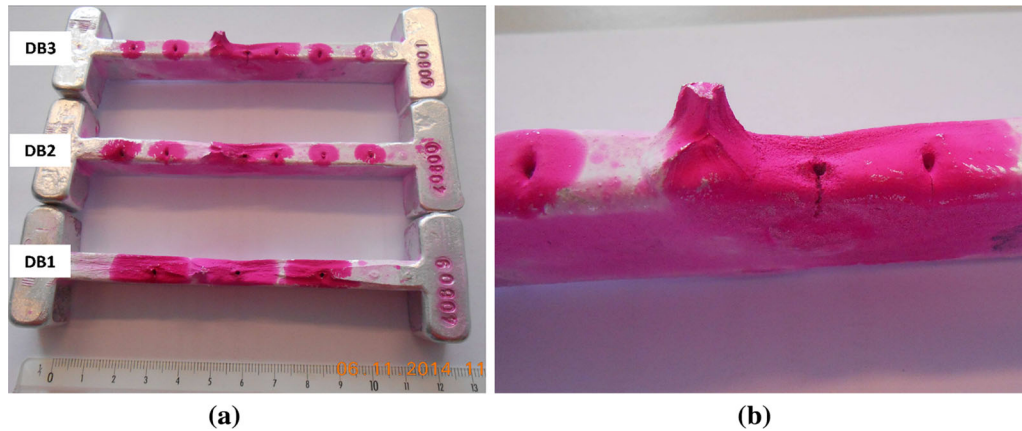


Fig. 2—(a) Dye penetrant tests on the three Al-Zn castings and (b) hot tear formed at the location of the central thermocouple in sample DB3.

The monochromatic 60.07 keV XRD patterns were acquired using a 2D flat panel detector covering a $426 \times 426 \text{ mm}^2$ area. The pixel size was $148 \mu\text{m}$ in each direction, and the sample-to-detector distance was 1299 mm, measured from the middle of the sample. The beam size was $0.5 \times 0.5 \text{ mm}$ and the sample thickness was 7.5 mm in the gage volume in order to minimize ring broadening. The acquisition of both temperature and diffraction patterns was synchronized and recorded at a continuous acquisition rate of 2 Hz.

III. RESULTS

A. Al-Zn Castings and Microstructure

Three dog-bone (DB)-shaped samples of identical length have been cast and named DB1, DB2, and DB3. Small hot tears were visible at the surface of DB1 and DB3. Dye penetrant tests conducted after the *in situ* diffraction experiment revealed that all three samples contained hot tears at the hot spot location as shown in

Figure 2(a). DB3 presented a crack at the location of the central thermocouple (*cf.* Figure 2(b)), which can promote initiating hot tears.^[1]

Figure 3 shows scanning electron microscopy (SEM) image of DB3. The secondary electron mode was used to see solute rich grain boundaries and intergranular microsegregation. The microstructure is globular as a result of both the use of grain refiner and a rather high cooling rate. An average grain size of $120 \mu\text{m}$ is determined, and the Al-Zn eutectic is clearly visible at grain boundaries meaning that the solidification ends with the eutectic transformation at 654 K (381 °C).^[21,22] Some micropores and incipient hot tears are also visible at triple grain junctions. Samples DB1 and DB2 exhibit a similar microstructure.

B. Temperature Measurements During Casting

Figure 4(a) shows the temperature recorded at the hot spot location for all three castings. The liquid metal temperature varied from 963 K to 1028 K (690 °C to

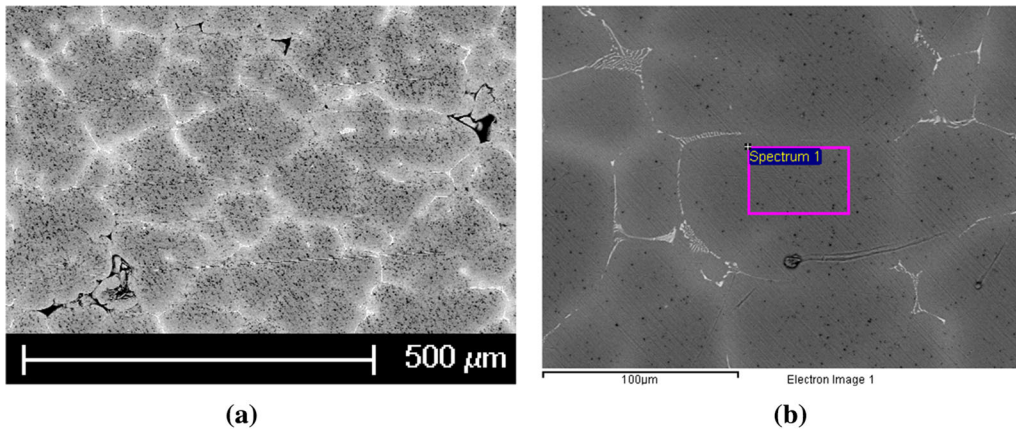


Fig. 3—(a) SEM micrograph of the Al-Zn sample DB3 using secondary electron mode and (b) zoom in region showing the formation of Al-Zn eutectic at grain boundaries.

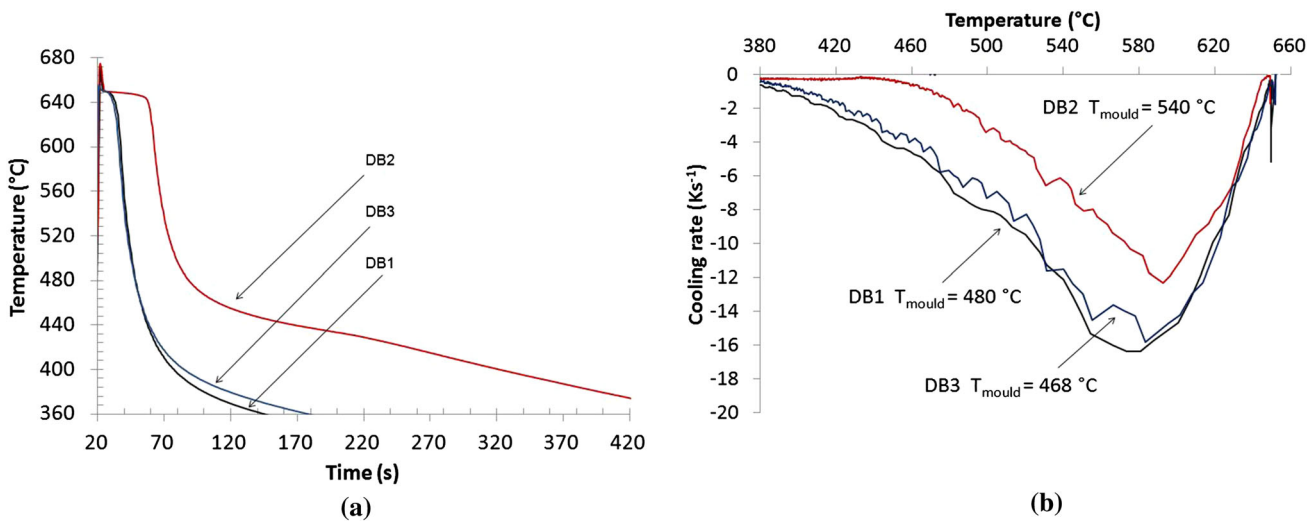


Fig. 4—(a) Temperature vs time at the hot spot for the three samples, (b) cooling rate as a function of temperature at the same location.

Table I. Experimental Conditions and Rigidity TEMPERATURE and Solid Volume Fraction for the Three Al-Zn Samples

Sample	Solidification Time (s)	Initial Mold Temperature	Average Cooling Rate (K/s)	Rigidity Temperature	g_s at Rigidity (pct)	Cooling Rate at Rigidity (K/s)
DB1	76	753 K (480 °C)	-3.6	829 to 839 K 556 to 566 °C	98.4	-16
DB2	363	813 K (540 °C)	-0.7	858 to 866 K 585 to 593 °C	97.4	-7
DB3	97	741 K (468 °C)	-2.8	829 to 839 K 556 to 566 °C	98.4	-12

755 °C) and the initial mold temperature from 713 K to 813 K (440 °C to 540 °C), thus having different cooling rates. DB1 and DB3 exhibit a similar cooling path, whereas DB2 solidifies with a lower cooling rate. As soon as the alloy starts to solidify, latent heat is released and the temperature exhibits a plateau. The liquidus temperature for each casting is given by this plateau and values around 923 K (650 °C) \pm 0.5°K are found indicating a Zn content of 6.2 wt pct according to Al-Zn phase diagram.^[21,22] Samples were prepared with 5 wt pct of Zn. This discrepancy is explained from macrosegregation taking place at the length scale of the

casting. Indeed, during casting solute cumulates ahead of the two solidification fronts advancing from both mold extremities enriching the liquid at the hot spot. Solidification times for the transition from liquidus and eutectic are comparable for DB1 and DB3 (76 and 97 seconds) but are much longer for DB2 (373 seconds). This is attributed to the lower initial mold temperature for these two castings, 753 K and 741 K (480 °C and 468 °C), compared with sample DB2, 813 K (540 °C). Figure 4(b) presents the cooling rate experienced by each sample as a function of the temperature at the hot spot. The cooling rate is almost nil at the liquidus

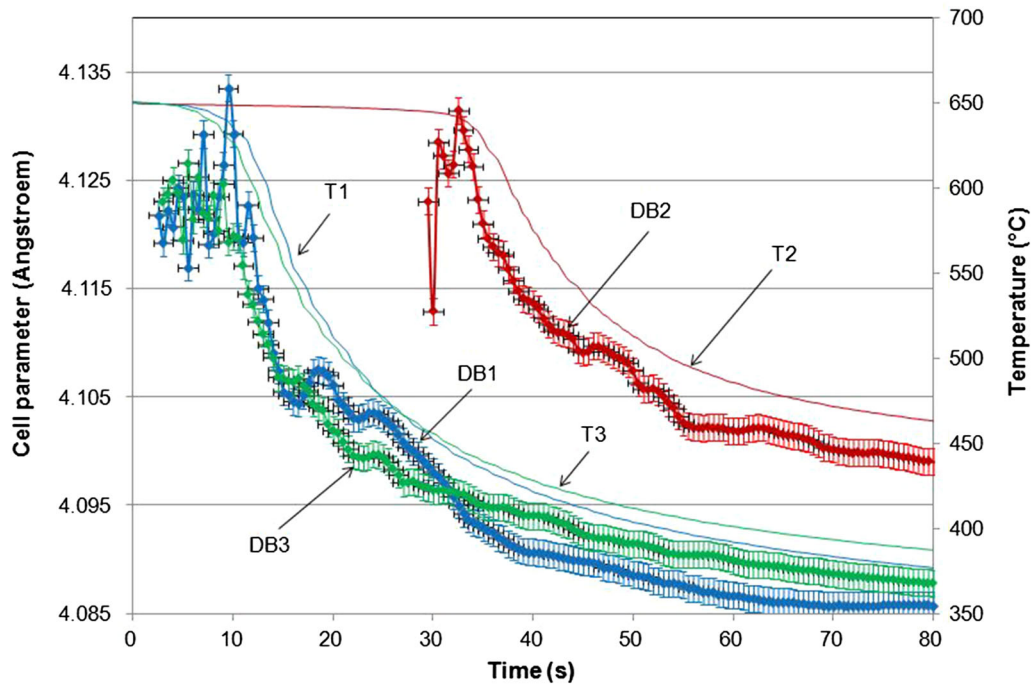


Fig. 5—Lattice parameter and temperature vs time at the hot spot for all samples.

temperature and reaches a maximum value around 853 K (580 °C). DB1 and DB3 exhibit similar cooling rates with a maximum value of about -16 K/s. Table I sums up the experimental conditions.

C. Diffraction Patterns

All diffraction patterns recorded during casting were integrated using DAWN software to reduce them to 1D patterns, and TOPAS Academic[®] to retrieve the lattice parameter, using CeO₂ powder as a calibration sample. This reduction to 1-dimensional data is justified for samples exhibiting isotropic strain, as is the case here. The lattice parameter of FCC aluminum solid solution at the hot spot located in the gage volume was extracted using Bragg's law. The high temporal resolution allowed us to obtain a sufficient number of diffraction peaks during solidification. The small beam size and small sample thickness yielded very clean diffraction peaks leading to weighted profile R-factor (Rwp) in the order of 15 pct using Le Bail fit^[23] and thus small error bars.^[24] With an average grain size of 120 μm and a gage volume of $0.5 \times 0.5 \times 7.5 \text{ mm}^3$, the number of irradiated grains is approximately 2'000 thus providing good statistics.

Figure 5 shows the evolution of the lattice parameter and temperature for three Al-Zn castings as a function of time taking the liquidus temperature as time reference. In all three samples, first diffraction peaks form a couple of degrees below the liquidus temperature. The lattice parameter exhibits first erratic evolution as grains are free to rotate and thus lose Bragg diffraction conditions. As temperature decreases, the lattice parameter decreases but small bumps appear in DB1 and DB3. Each of those bumps is well defined by many diffraction points. For DB2, such bumps are also visible, *e.g.*, at

813 K (540 °C), but less pronounced and disappear with further temperature decrease.

IV. DISCUSSION

A. Solidification Path and Evolution of Lattice Parameter During Solidification

The temperature evolution of the sample during casting and the digitized Al-Zn phase diagram,^[21] shown in Figure 6(a), have been used to calculate the volume fraction of solid, g_s , during solidification. The eutectic temperature is 654 K (381 °C) with a Zn content of 95 wt pct in the liquid phase. Using the Zn diffusion coefficient in the solid aluminum phase given by Y. Du *et al.*^[25] and the measured solidification times, the mean diffusion length, around 6 μm in samples DB1 and DB3 and 10 μm in DB2, remains small compared with the mean grain radius, 60 μm , thus justifying the use of the Scheil-Gulliver model to calculate the solidification path, *i.e.*, the solid fraction vs temperature. The assumptions of this approach are that solute concentration at the solid liquid interface is given by the equilibrium phase diagram, no solute diffusion occurs in the solid phase and perfect solute mixing exists in the liquid phase.^[1] As the partition coefficient which is the ratio of the concentration at liquidus and solidus is not constant during solidification (*cf.* Figure 6(b)), the Scheil-Gulliver equation cannot be used directly. To overcome this problem, the liquidus and solidus lines have been tabulated and the solidification path has been calculated incrementally using the Scheil-Gulliver assumptions. The evolution of the fraction of solid, g_s , in this case is given by [1]:

$$(c_1^* - c_s^*)dg_s = (1 - g_s)dc_1^*, \quad [1]$$

where c_1^* and c_s^* are the liquidus and solidus Zn concentration at the solidification front. Figure 6(b) shows the calculated solid fraction v_s vs temperature for the Al-Zn 6.2 wt pct owing to macrosegregation. Solidification starts at 923 K (650 °C) and ends up at 654 K (381 °C) with a very small fraction of eutectic, *i.e.*, 0.15 pct, in accordance with the microstructural observations (*cf.* Figure 3). It should be noticed that g_s increases very rapidly at the beginning of solidification and reaches 90 pct at 907 K (634 °C). Then solidification proceeds slowly to finish at the eutectic temperature. This part of the curve is crucial to determine the solid fraction at mechanical coherency.

The FCC aluminum solid solution lattice parameter is dependent on solute content, temperature, and strains. The solutal contribution to the lattice parameter is averaged over all the grains growing in the gage volume. It can be assessed by calculating the Zn composition assuming that all grains nucleate at the hot spot simultaneously at the liquidus temperature owing to the use of grain refiner. As shown in Figure 3, grains can

be assumed to grow as spheres of radius r with a final radius equal to the mean grain radius, $R = 60 \mu\text{m}$. The volume solid fraction is related to the grain radius by

$$g_s = \left(\frac{r}{R}\right)^3. \quad [2]$$

Figure 7(a) shows the Zn concentration profile during solidification as a function of the radius. This profile does not change with time as according to Scheil–Gulliver assumptions, *i.e.*, no solute diffusion in the solid and infinite solute diffusion in the liquid. Notice that the last layer of the solid forms at the eutectic Zn composition, *i.e.*, 85 wt pct. The mean Zn content within the solid phase during solidification, $C(r)$, is calculated using

$$C_{\text{Zn}}(r) = \frac{1}{\left(\frac{4\pi r^3}{3}\right)} \int_0^r 4\pi r^2 c(r) dr. \quad [3]$$

This quantity is presented in Figure 7(a). It increases from 3.37 wt pct at the very beginning of solidification

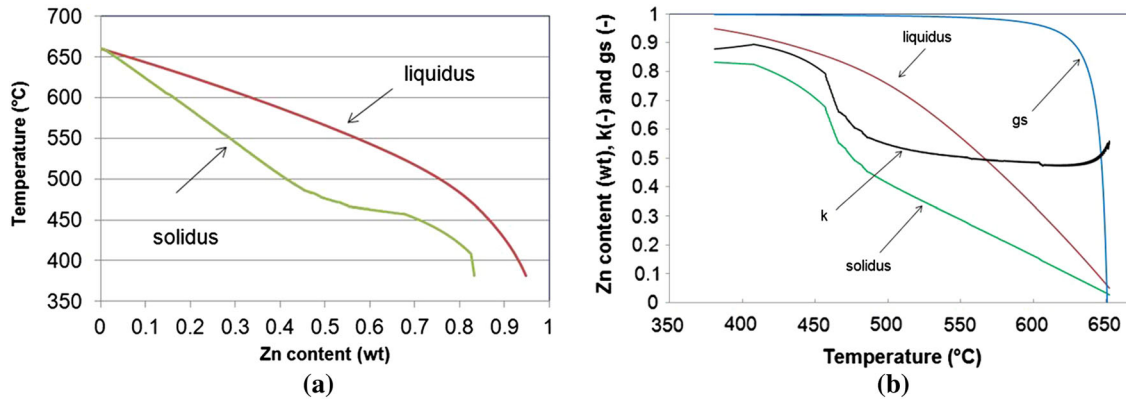


Fig. 6—(a) Equilibrium liquidus and solidus temperatures as a function of Zn content, (b) liquidus and solidus Zn concentration, solid fraction, g_s , and partition coefficient, k , as a function of temperature in Al-Zn 6.2 wt pct alloys.

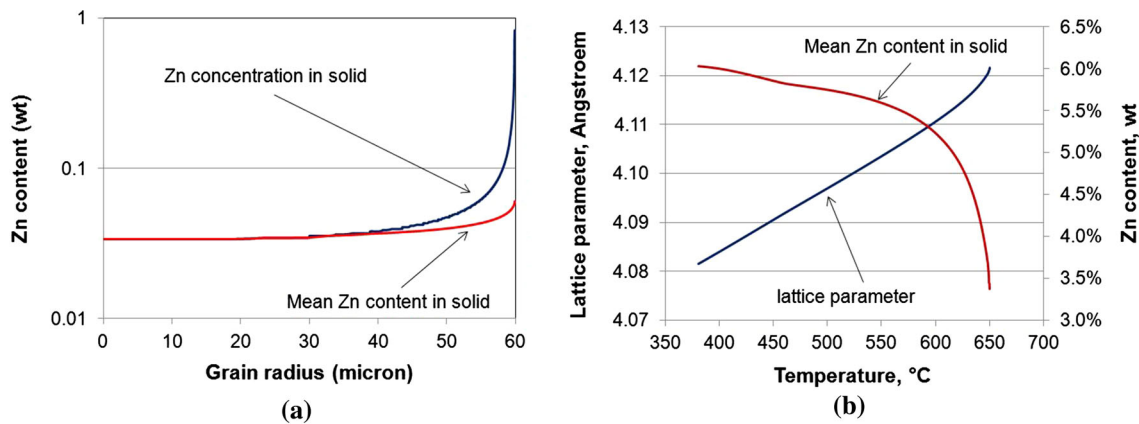


Fig. 7—(a) Zn concentration in the solid and mean Zn content in the solid vs the grain radius, (b) lattice parameter and mean Zn content in the solid as a function of temperature in the absence of macroscopic strains.

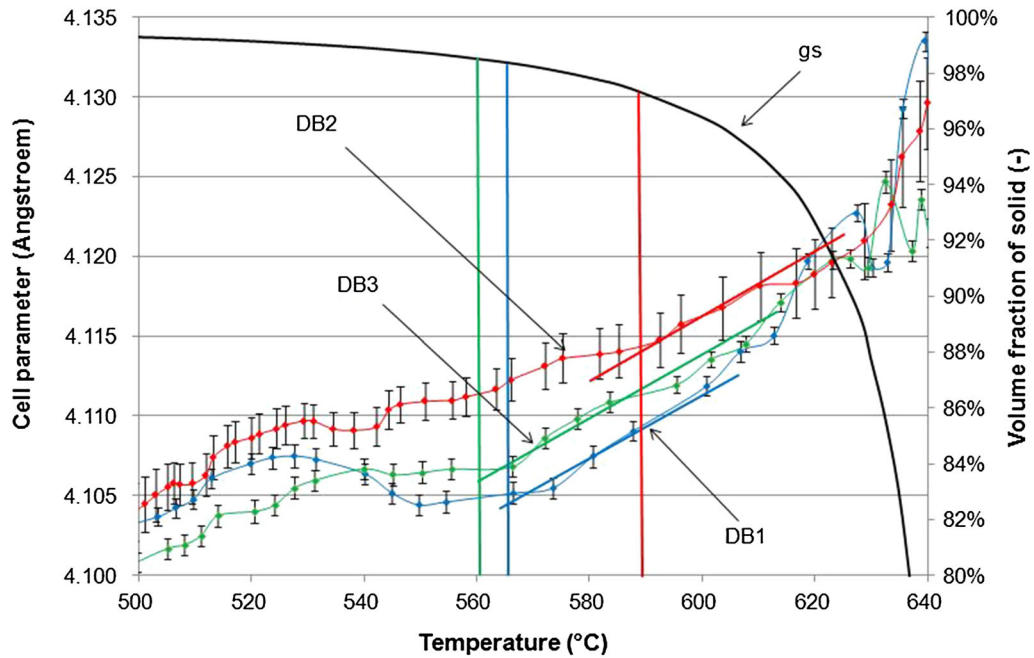


Fig. 8—Cell parameter and volume fraction of solid for the three samples vs temperature. Rigidity temperatures are schematically drawn for each sample.

and reaches 6.1 wt pct when solidification completes. As long as the solidifying alloy does not transmit macroscopic strains and stresses, the aluminum solid solution lattice parameter, a , is made of a thermal and a solutal contribution and can be written as

$$a = a_0(1 + \alpha_t(T - T_{\text{liq}}) + \alpha_s(C_{\text{Zn}}(r) - C_{\text{Zn}}^0)), \quad [4]$$

where α_t and α_s are the thermal and solutal coefficients, respectively, and a_0 is the lattice parameter of the very first crystals that form at the liquidus temperature, T_{liq} , with a Zn content, $C_{\text{Zn}}^0 = 3.37$ wt pct. The lattice parameter calculated with Eq. [4] for the Al-Zn 6.2 wt pct is drawn as a function of temperature in Figure 7(b) using $\alpha_t = 35 \times 10^{-6}/\text{K}$, a typical value for aluminum alloys at high temperatures, and $\alpha_s = -0.08/\text{wt. Zn}$ taken from.^[23] In the absence of any strains/stress during solidification, both contributions tend to decrease the lattice parameter, as shown in Figure 7(b). The solutal contribution is mainly present at the early stages of solidification, where the mean Zn content in the grain increases rapidly between 923 K and 873 K (650 °C and 600 °C). The steep decrease in the lattice parameter right below the liquidus temperature is explained by the rapid increase of the mean Zn content in the solid. With the *in situ* XRD measurements, the lattice parameter is expected to exhibit such a behavior as long as individual grains or grain clusters grow without transmitting any macroscopic tensile strains.^[26,27] At mechanical coherency, solid bridges are well established between grains and grain clusters and macroscopic strains and stresses start to develop possibly leading to the formation of micropores and hot tears, as reported in Figure 3.

B. Determination of Rigidity Temperature and Solid Volume Fraction

During its decrease, the lattice parameter reported in Figure 5 exhibits small deviations or bumps that are well defined by many diffraction points. These bumps are associated with the formation and coalescence of grain clusters as reported by Vernède *et al.*^[26] and Sistaninia *et al.*^[27] As soon as those grain clusters tend to weld together, macroscopic tensile strain develops owing to the constrained configuration of the dog-bone-shaped casting and leads to the formation of hot tears as shown in Figure 3. Stresses and strains are then relaxed and the lattice parameter continues to decrease. Hot tears might be healed by liquid or propagate within the casting. The scenario repeats until the load bearing surface is sufficiently reduced by the presence of hot tears.

Using Eq. [1], the solidification path is calculated for the Al-Zn 6.2 wt pct alloy. The solid fraction is shown in Figure 8 together with the evolution of the lattice parameter for g_s greater than 0.8. At such solid volume fractions, the solutal contribution to the lattice parameter becomes negligible (*cf.* Figure 7(b)) and only the thermal contribution remains as long as each individual grain or grain cluster is free to contract, *i.e.*, does not undergo macroscopic straining. In that case, the lattice parameter decrease with temperature is linear with a slope equal to α_t . Such linear decrease is shown in Figure 8 using $\alpha_t = 35 \times 10^{-6}/\text{K}$ for all three samples. When the lattice parameter starts to deviate from this linear decrease, the hot spot undergoes macroscopic straining associated with the dog-bone configuration. At that moment, grains and grain clusters have sufficiently coalesced to transmit tensile strains and stresses. Rigidity or mechanical

coherency is reached and temperature and solid volume fraction are determined using the three vertical lines. The results are cumulated in Table I with experimental conditions for each sample. In sample DB2, the rigidity temperature is 862 K (589 °C) \pm 4 K and corresponds to a solid volume fraction of 97.4 pct. For other two samples, rigidity takes place later at lower temperatures, 834 K (561 °C) \pm 5 K, corresponding to a solid volume fraction around 98.4 pct. The lower rigidity temperature found in samples DB1 and DB3 is explained by the lower solidification time, 76 and 97 seconds compared with 363 seconds in sample DB2, and the associated higher cooling rate. Time for coalescence is limited and thus mechanical coherency is delayed. The volume fraction of solid at rigidity determined in the present work agrees with recent studies on tensile coherency^[4] and hot tearing^[28] in aluminum alloys. The dependence with solidification time is also in accordance with the industrial observation that increasing casting speed during DC casting of aluminum billets and rolling sheets increases drastically the risk of hot tearing.^[1]

V. CONCLUSIONS

Mechanical coherency and hot tears formation have been observed in Al-Zn 6.2 wt pct alloys using *in situ* XRD during casting in a dog-bone-shaped mold. With a time resolution of 0.5 seconds, the evolution of the solid aluminum lattice parameter reveals small deviations at high solid volume fractions which are explained by the accumulation of macroscopic strains and stresses that are relaxed by the nucleation of micropores and hot tears. Rigidity temperature and solid volume fraction are determined by the instant when the lattice parameter starts to deviate from its linear decrease as the solute contribution to the lattice parameter becomes negligible at such high solid fractions. Rigidity depends on solidification time. The volume fraction of solid at rigidity increases from 97.4 pct with a solidification time of 363 seconds to 98.4 pct with solidification times around 86 seconds. These findings are in good agreement with previous studies on coalescence and hot tearing in aluminum alloys and should be extended to industrial alloys and shorter solidification times using a higher time resolution.

ACKNOWLEDGMENTS

The authors express their deep acknowledgements to the Swiss National Science Foundation, Bern, for funding (Project No. 200021_146879) and the Diamond Light Source, Oxfordshire, UK, for the provision of beam time.

REFERENCES

1. J.A. Danzig and M. Rappaz: *Solidification, Defects*, EPFL Press, Lausanne, Switzerland, 2009.
2. M. Rappaz, A. Jacot, and W.J. Boettinger: *Metall. Mater. Trans. A*, 2003, vol. 34A, pp. 467–79.
3. J.-M. Drezet, B. Mireux, Z. Szaraz, and T. Pirling, *Materials* 2014, vol. 7, pp. 1165–72, <http://www.mdpi.com/1996-1944/7/2/1165>.
4. S. Li, K. Sadayappan, and D. Apelian: *Int. J. of Cast Metal Res*, 2011, vol. 24 (2), pp. 88–95.
5. M. Rappaz, J.-M. Drezet, and M. Gremaud: *Metall. Mater. Trans. A*, 1999, vol. 30A, pp. 449–55.
6. A. Stangeland, A. Mo, M. M'Hamdi, D. Viano, and C. Davidson: *Metall. Mater. Trans. A*, 2006, vol. 37A, pp. 705–14.
7. S. Terzi, L. Salvo, M. Suery, N. Limodin, J. Adrien, E. Maire, Y. Pannier, M. Bornert, D. Bernard, and M. Felberbaum: *Scripta Mater.*, 2009, vol. 61, pp. 449–52.
8. Suéry, M.; Terzi, S.; Mireux, B.; Salvo, L.; Adrien, J.; Maire, E. Fast, *JOM* **2012**, *64*, 83–88.
9. A.B. Phillion, R.W. Hamilton, D. Fuloria, A.C.L. Leung, P. Rockett, T. Connolley, and P.D. Lee: *Acta Mater.*, 2011, vol. 59, pp. 1436–44.
10. C.M. Gourlay, A.K. Dahle, T. Nagira, N. Nakatsuka, K. Nogita, K. Uesugi, and H. Yasuda: *Acta Mater.*, 2011, vol. 59, pp. 4933–43.
11. E. Giraud, M. Suéry, and M. Coret: *Metall. Mater. Trans. A*, 2010, vol. 41A, pp. 2257–68.
12. N. Limodin, L. Salvo, E. Boller, M. Suéry, M. Felberbaum, S. Gailliègue, and K. Madi: *Acta Mater.*, 2009, vol. 57, pp. 2300–10.
13. S. Terzi, J.A. Taylor, Y.H. Cho, L. Salvo, M. Suéry, E. Boller, and A.K. Dahle: *Acta Mater.*, 2010, vol. 58, pp. 5370–80.
14. J.-M. Drezet, A. Evans, T. Pirling, and B. Pitié: *Int. J. Cast Met.*, 2012, vol. 25, pp. 110–16.
15. Chobaut N., Reppe J., Pirling T., Carron D. and Drezet J.-M.: in *13th International Conference on Aluminum Alloys (ICAA13)*, H. Weiland, A.D. Rollett, and W. A. Cassada, eds., TMS (The Minerals, Metals & Materials Society), 2012, 285–291.
16. J.S. Robinson *et al.*: *Mater. Sci. Technol.*, 2012, vol. 28 (4), pp. 420–30.
17. W. Woo, Z. Feng, X.-L. Wang, D.W. Brown, B. Clausen, K. An, H. Choo, C.R. Hubbard, and S.A. David: *Sci. Technol. Weld. Join.*, 2007, vol. 12 (4), pp. 298–303.
18. Diamond Light Source, Oxfordshire, UK, JEEP web site <http://www.diamond.ac.uk/Beamlines/Engineering-and-Environment/I12.html>.
19. M. Sistaninia, J.-M. Drezet, A.B. Phillion, and M. Rappaz: *JOM*, 2013, vol. 65 (9), pp. 1131–37.
20. M. Lalpoor, D.G. Eskin, and L. Katgermann: *Metall. Mater. Trans. A*, 2009, vol. 40A, pp. 3304–13.
21. Alloy phase diagrams, ASM Handbook, vol. 3, ASM, 1992.
22. K.G. Satyanarayana: *J. Mater. Sci.*, 1981, vol. 16, pp. 1240–48.
23. A. Le Bail, H. Duroy, and J.L. Fourquet: *Mater. Res. Bull.*, 1988, vol. 23, pp. 447–52.
24. B.H. Toby: *J. Mater. Sci.*, 1981, vol. 16, pp. 1240–48.
25. Y. Du, Y. Chang, B. Huang, W. Gong, Z. Jin, H. Xu, Z. Yuan, Y. Liu, Y. He, and F. Xie: *Mater. Sci. Eng. A*, 2003, vol. 363, pp. 140–51.
26. S. Vernède, P. Jarry, and M. Rappaz: *Acta Mater.*, 2006, vol. 54, pp. 4023–34.
27. M. Sistaninia, A.B. Phillion, J.-M. Drezet, and M. Rappaz: *Acta Mater.*, 2012, vol. 60, pp. 3902–11.
28. A. Nordmark, K. Ellingsen, A. Johansson, M. M'Hamdi, A. Kvithyld, A. Marson, and A. Azar: *Mater. Sci. Forum*, 2014, vols. 794–796, pp. 95–100.